Al-Nahrain Journal for Engineering Sciences **NJES** 27(4)465-472, 2024
http://doi.org/10.29194/NJES.27040465

Automated Detection and Visualization of Local Kidney Images with Artificial Intelligence Models

Hawraa S. Saleh[1], Hadeel K. Aljobouri[2], Hani M. Amasha[3]

Authors affiliations:
1) Department of Computer Engineering, College of Engineering, Al-Nahrain University, Baghdad, Iraq.
hawraa0sattar@gmail.com

2*) Department of Biomedical Engineering, College of Engineering, Al-Nahrain University, Baghdad, Iraq.
hadeel.k.aljobouri@nahrainuniv.edu.iq

3) Biomedical Engineering Department, FMEE, Damascus University, Damascus, Syria
Hani.amasha@damascusuniversity.edu.sy

Paper History:

Received: 14th June 2024

Revised: 1st Aug. 2024

Accepted: 23rd Aug. 2024

Abstract

Kidney disease is a global health concern, often leading to kidney failure and impaired function. Artificial intelligence and deep learning have been extensively researched, with numerous proposed models and methods to improve kidney disease diagnosis. This work aims to enhance the efficiency and accuracy of the diagnostic system for kidney disease by using Deep Learning, thereby contributing to effective healthcare delivery. This work proposed three models: CNN, CNN-XGBoost and CNN-RF to extract features and classify kidney Ultrasound images into four categories: three abnormal cases (stones, hydronephrosis, and cysts) and one normal case. The models were tested on a real dataset of 1260 kidney ultrasound images (from 1000 patients) collected from the Lithotripsy Centre in Iraq. CNN models are often viewed as black boxes due to the challenge of understanding their learned behaviors, Visualizing Intermediate Activations (VIA) was used to address this issue. The proposed framework was assessed based on precision, recall, F1-score, and accuracy. CNN-RF is the most accurate model, with an accuracy of 99.6%. This study can potentially assist radiologists in high-volume medical facilities and enhance the accuracy of the diagnostic system for kidney disease.

Keywords: CNN, Deep Learning, Feature Extraction, Kidney Diseases, RF, Ultrasound Images, Visualization.

الكشف الآلي وتصور صور الكلى المحلية باستخدام نماذج الذكاء الاصطناعي

حوراء ستار صالح ، هديل قاسم وادي الجبوري، هاني عماشة

الخلاصة:

أمراض الكلى هي مشكلة صحية عالمية تؤدي غالبًا إلى الفشل الكلوي وضعف وظائف الكلى. لقد تم إجراء العديد من البحوث حول الذكاء الاصطناعي والتعلم العميق، مع اقتراح العديد من النماذج والأساليب لتحسين تشخيص أمراض الكلى. يهدف هذا العمل إلى تحسين كفاءة ودقة نظام التشخيص لأمراض الكلى باستخدام التعلم العميق، مما يساهم في تقديم الرعاية الصحية الفعالة. اقترح هذا العمل ثلاثة نماذج: شبكة CNN، وشبكة CNN-XGBoost، وشبكة CNN-RF لاستخراج الخصائص وتصنيف صور الموجات فوق الصوتية للكلى إلى أربع فئات: ثلاث منها حالات غير طبيعية (الحصوات، تضخم الكلية، الخراجات) وحالة طبيعية واحدة. تم اختبار النماذج على مجموعة بيانات حقيقية مكونة من ١٢٦٠ صورة الموجات فوق الصوتية للكلى (من ١٠٠٠ مريض) تم جمعها من مركز تفتيت الحصى في العراق. غالبا ما ينظر إلى نماذج الCNN على أنها صناديق سوداء بسبب التحدي المتمثل في فهم سلوكياتهم المكتسبة، تم استخدام تصور عمليات التنشيط الوسيطة (Visualizing Intermediate) لغرض معالجة هذه المشكلة. تم تقييم النماذج المقترحة بناء على(precision, recall, F1-score, accuracy). يعد نموذج CNN-RF النموذج الأكثر دقة حيث تبلغ دقته ٩٩,٦٪. يمكن أن تساعد هذه الدراسة أخصائي الأشعة في المرافق الطبية عالية الكثافة وتحسين دقة نظام التشخيص لأمراض الكلى.

1. Introduction

Renal diseases involve gradual loss of renal function in filtering metabolic wastes and blood fluids, kidney diseases include kinematic damage, kidney cysts, kidney stones, hydronephrosis, and other kidney infections [1]. Accounting shows that kidney diseases

caused 1.34 and 1.36 million deaths in the years 2021 and 2022, according to the World Health Organization. Kidney diseases were Iraq's main cause of death in 2022, with 26,000 fatalities and 25,000 deaths in 2021. Kidney diseases include stones that are concretions that materialize in the presence of elevated concentrations of calcium, oxalate, cystine, or phosphate and insufficient fluid [2]. Accumulation of crystals in the kidney regions, known as nephrolithiasis, leads to renal failure in advanced stages [3]. Cystic renal disease is a pathological state distinguished by the existence of multiple fluid-filled cysts within the renal tissue. These cysts exert pressure on the nephrons responsible for regulating kidney function, resulting in renal failure [4]. Obstructive hydronephrosis is the term used to describe anatomical and functional problems with the kidneys brought on by obstructions in the urine's flow, which makes it difficult to urinate [5]. Hematepuria and the presence of hydronephrosis on ultrasound imaging can be valuable indicators of renal colic. [6]. Ultrasound imaging, known as sonography, high-frequency sound waves are employed to diagnose soft tissues like muscles and internal organs, including kidney diagnosis [7], [8]. Renal ultrasound (US) is a preferred imaging modality because of a safe, non-invasive, and cost-effective test, US is a useful tool for making medical decisions [9].

Artificial intelligence (AI) and DL play crucial roles in healthcare, particularly in diagnosing various diseases [10], [11]. AI is a branch of computer science that can be applied to design software models that can imitate human tasks [12], [13]. Deep-learning technology is a branch of machine learning that uses multiple artificial neurons to identify intricate features in input datasets, addressing complex real-world issues [14], [15].

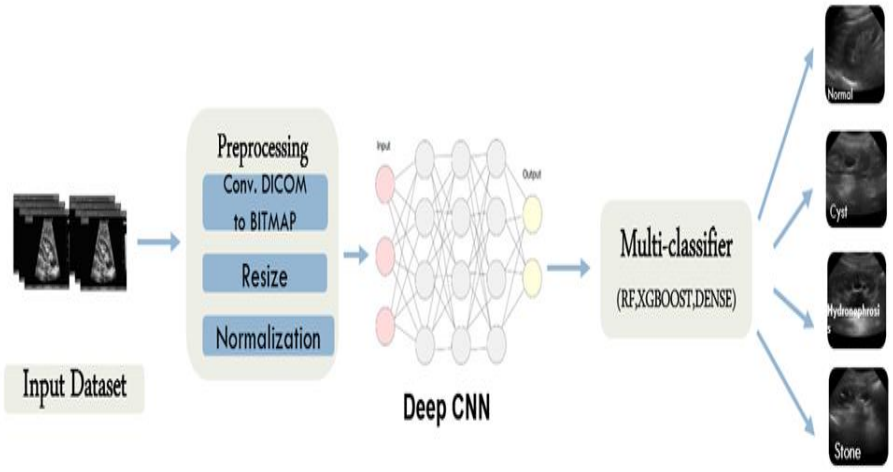

Figure (1): Processing diagram for the suggested methods.

AI and deep learning for better-diagnosing kidney diseases have been widely researched with many proposed models and methods [16], [17]. In 2019 ResNet-100 and XGboost were used for the binary classification of 4,505 kidney ultrasound images, achieving an accuracy of 85.6% [18]. Kokil and Sudharson [19] proposed a two-stage approach for classifying kidney abnormalities in ultrasound images. first, a pre-trained convolutional neural network (CNN) was utilized to extract relevant features from the images. Then, SVM was employed to classify the extracted features into three categories: normal, cystic, and stoned. In 2020, Sudharson and Kokil developed an approach ensemble ResNet-101, Shuffle Net, and MobileNet-v2 models to extract features (from 4940 kidney US images), an SVM employed to classify the images into four classes (normal, cyst, stone, and tumour). The method achieved an accuracy of 96.54% [20]. In 2023 Raja Sankari Vm et al. suggested a custom CNN model to classify 1000 US images into binary classes, with a classification accuracy of 95% [21].

In this work, the CNN model was employed to extract features, fully connected layers, RF and XGboost algorithms were used to classify kidney ultrasound images into four classes (normal, stone, hydronephrosis, and cysts), the Visualizing Intermediate Activations (VIA) was used to understand the CNN layers. The models were trained and tested on ultrasound images of kidneys collected from the Lithotripsy Centre in Iraq. The major contributions of this work are:

A computer-aided diagnosis system based on a DL model to enhance the accuracy of kidney disease classification from normal.

A CNN extracted features from the ultrasound images. These features were fed into fully connected layers, XGBoost and Random Forest algorithms for multiclassification tasks.

2. Methodology

The process of the proposed models is illustrated in Figure 1. The preprocessing and data collecting are the two primary aspects of this section. In the next paragraphs, the details of these sections are presented.

3. The Dataset Collection

For this research, real kidney ultrasound datasets were obtained from the Lithotripsy Center at Al-Diwaniyah General Teaching Hospital, Iraq. The images were acquired using a Philips HD11 XE ultrasound system, which produces images in DICOM format with a resolution of 800x600 pixels. The dataset of images was diagnosed by three urologists and one radiologist and categorized into four categories: normal, cyst, hydronephrosis, and stone. Obtained four cases a total of 1260 US images from 1000 patients (cyst, stone, hydronephrosis, and normal), 315 US images were collected for each class. Figure (2) displays three classes of kidney disease and the normal case and presents the region of interest (ROI).

4. Preprocessing

The preparation of data is crucial in medical imaging. Pre-processing is frequently necessary to do significant data analysis. In this work, pre-processing is done in four steps: normalization, scaling, cropping, and the format of the image. Image format, the images were preprocessed to prepare them for the feature extraction step. First of all, the images that were collected, were converted from DICOM to BITMAP. After that, the images are organized and separated randomly into 80% for training (1008 images) and 20% for testing (252 images).

In the image resizing the size of the images was changed to a new size (224 x 224). It is preferable to resize all images to a uniform size, and standard image dimensions for CNN training often fall between 64 × 64 and 256 × 256 [22] [23]. Then Normalize the values of pixels from a resolution range of (0- 255) to a range of (0 - 1) to obtain neural networks that operate with small input values [24]. It is recommended for neural network-based classification methods [25].

5. The Proposed Models:

5.1 Feature Extractions

Deep learning involves feature extraction, identifying meaningful patterns from pre-processed data to enhance model performance in tasks like classification, object detection, and image segmentation [26]. There are several techniques for that purpose deep CNNs are the primary method for feature extraction in AI, employing convolutional layers, pooling layers, and activation functions to extract low-level features, reduce spatial resolution, and learn complex relationships [27]. This work used CNN model to extract features from kidney US images.

5.1.1 CNN

CNN is a prominent algorithm in deep learning methods and has been used in various applications such as image processing, classification, and enhancement tasks [28][29]. The proposed CNN architecture consists of three convolution layers each followed by MaxPooling layers and an activation function (Relu). Following the last convolutional block, a flattened layer was used to keep the output of convolution layers into a one-dimensional vector, the dense layer's (fully connected layers) classify the images into four classes, The CNN structure with dense layers is illustrated in Figure (3**).**

5.2 Classification

The computational complexity of the model is decreased by the image classification algorithms. Classifying images from numerous modalities to discriminate between different disease types of biomarkers is the ultimate goal of medical imaging analysis [30]. In this work, extracted features were fed into fully connected layers or to machine learning algorithms: FC, XGBoost and RF to classify kidney US images. The models predict four classes with the highest probability based on the learned features.

5.2.1 Fully Connected Layer

Classification layers mainly include the Fully connected (FC) layers also referred to as a dense layer [31]. The proposed CNN architecture was used to extract features, dense layers (fully connected layers) with SoftMax activation function classify the images into four classes, The CNN structure with dense layers is illustrated in **figure (3).**

5.2.2 XGBoost

Extreme Gradient Boosting (XGboost) is a decision tree-boosting model developed by Chen et al. [32]. XGBoost can handle continuous features by dividing them into buckets during training. It considers the distribution of data points within each bucket to find optimal split points for decision trees. Each iteration of XGBoost adds a new decision tree to the ensemble, focusing on improving the model's performance based on a specific loss function. XGBoost objective function is the sum of the regularization function for every prediction (K trees) and the loss function computed over the entire set of predictions.

$$Obj = \sum_i^n l(y_i, \hat{y}) + \sum_{k=1}^K \Omega(f_k) \quad \ldots(1)$$

Where (y_i, y) the training loss determines how the model fits the training data, Ω regularization measures the complexity of trees, and K is the number of trees. The proposed CNN-XGBoost architecture consists of three convolution layers each followed by MaxPooling layers and an activation function (Relu). following the last convolutional block, a flattened layer was used to keep the output of convolution layers into a one-dimensional vector, the dense layers (fully connected layers) were eliminated, and then the XGBoost was added classified the extracted features. The structure of the CNN-XGBoost model was illustrated in Figure (4).

5.2.3 RF

The ensemble learning classification algorithm Random Forest (RF) is a potent tool with large training datasets and numerous input variables. It is frequently used in situations with small sample sizes, such as the analysis of gene expression data [33]. The primary benefit of RF is that it improves forecast accuracy without increasing computing expenses. The method's essence is building multiple trees in randomly selected subspaces of the feature set. Different subspaces of trees extend the classification in distinctive ways. Their general classification can be gradually enhanced [34]. In this work, the performance of the RF was created using 100 estimators trained with the CNN model. The proposed CNN-RF architecture consists of three convolution layers each followed by MaxPooling

layers and an activation function (Relu). following the last convolutional block, a flattened layer was used to keep the output of convolution layers into a one-dimensional vector, the dense layers (fully connected layers) were eliminated, and the RF classified the extracted features. The structure of the CNN-RF model is illustrated in Figure (5).

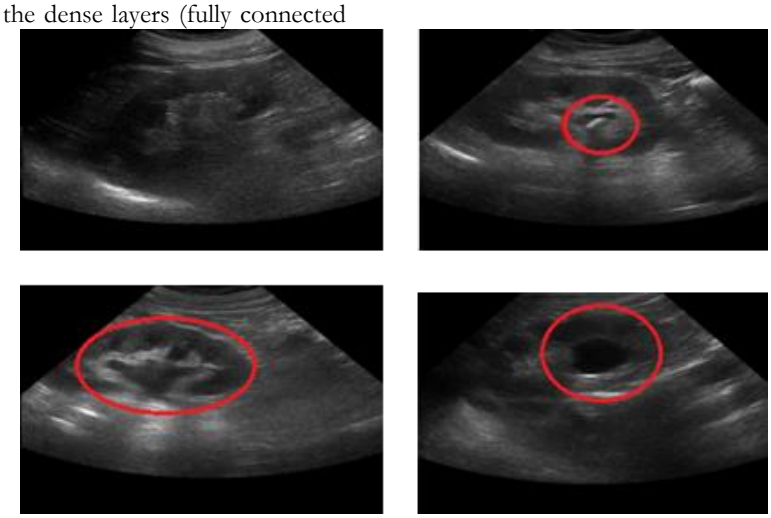

Figure (2): Samples of kidney US images: (a) Normal, (b) Stone, (c) Hydronephrosis, (d) Cysts.

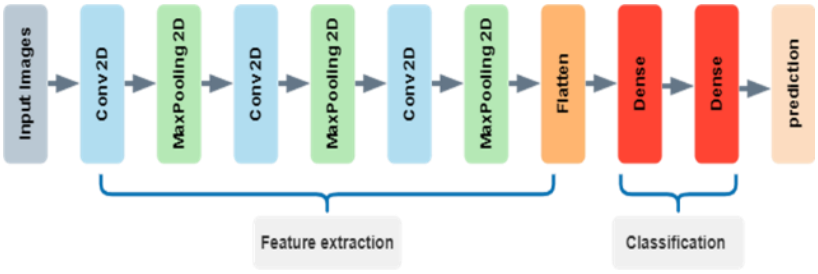

Figure (3): The structure of the CNN model

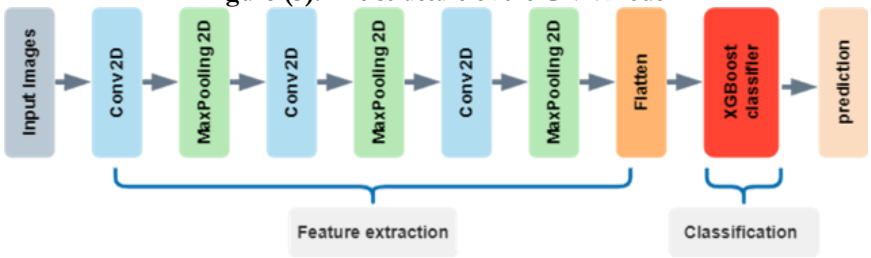

Figure (4): The structure of the CNN-XGBoost model.

5.3 Visualizing Intermediate Activations (VIA) in CNN

CNN models are often considered black boxes due to the challenge of understanding their learned behaviors, VIA was proposed to address this issue [35]. These visualizations, known as feature maps, reveal how the network progressively extracts and refines features from the input image as it passes through the convolutional layers [36]. The CNN model was loading and the kidney US image was used after preprocessing for visualizing the layers of CNN model activations. Figure (6) shows the process of VIA for the convolutional layers of CNN models.

6. Results:

The experiments were all run on an ASUS laptop with a 12th gen Intel Core i7 processor (2.30 GHz) and 64-bit operating system. Python tool version 3.10.7 is used. The installation of the software program included: Anaconda Navigator, Spyder, and Python.This study uses the CNN model to extract features from 1260 kidney ultrasound images. The kidney US images were classified into four categories: FC, XGboost and RF. The proposed models are assessed utilizing a hold-out (80%–20%) train–test splits, the reason for this split ratio coming from effectiveness in various scenarios, providing a balance between training and unbiased evaluation. It reduces the computational cost, especially for large datasets, and is straightforward to implement. The comparison results indicate that the accuracy of the classification was 99% for CNN-RF and 99.6% for CNN-XGBoost. This shows that the CNN-XGBoost model has a better performance. Figure (7) shows the accuracy and loss curves of the CNN model, having a total of 20 epochs. The confusion matrix in Figure (8) summarizes the model's performance on the four kidney US image classes. The x-axis represents the predicted class, and the y-axis represents the actual class.

True Negative (TN), True Positive (TP), False Negative (FN), and False Positive (FP) values are calculated using the following formula:

$$Accuracy=(TP+TN)/(TP+FP+FN+TN) \quad (2)$$

$$Precision=TP/(TP+FP) \quad (3)$$

$$Recall=TP/(TP+FN) \quad (4)$$

$$F1score = ((2 \times (Recall \times Precision))/(Precision + Recall) \quad (5)$$

The proposed method is assessed for accuracy, precision, specificity, sensitivity and F1 score to evaluate the applicability. The performance of CNN models is shown in Tables 1,2 and Table 3.

To better understand the CNN model's functionality and learned behaviors, the activations of it intermediary layers were visualized. To visualize the activations in an input picture of kidney US, random filters were derived from the feature maps and displayed, as Figure (9) illustrates. With the depth of the layer, the sparsity of activations increased: in the first convolutional layer, the input picture activated nearly every channel; in the later layers, many of the channels were blank, indicating that the pattern these filters were encoding was not present in the input image. As a result, CNN was able to grasp the significant, universal feature of the representations, which was that features become more abstract as the layer got deeper. Deeper layer activations conveyed additional details about the US imaging modalities as well as nuanced information about the particular input being viewed.

Table (1): Performance of the CNN model (80%–20% train–test split).

Class	Precision	Recall	F1 score	Support	accuracy
Stone (0)	100%	100%	100%	67	97%
Normal (1)	94%	94%	94%	67	
Hydronephrosis (2)	100%	98%	99%	58	
Cysts (3)	93%	95%	94%	60	

Table (2): Performance of the CNN-XGBoost model (80%–20% train–test split)

Class	Precision	Recall	F1 score	Support	Accuracy
Stone (0)	100%	100%	100%	67	99%
Normal (1)	99%	99%	99%	67	
Hydronephrosis (2)	100%	100%	100%	58	
Cysts (3)	98%	98%	98%	60	

Table (3): Performance of the CNN-RF model (80%–20% train–test split).

Class	Precision	Recall	F1 score	Support	Accuracy
Stone (0)	100%	100%	100%	67	99.6%
Normal (1)	99%	100%	99%	67	
Hydronephrosis (2)	100%	100%	100%	58	
Cysts (3)	100%	98%	99%	60	

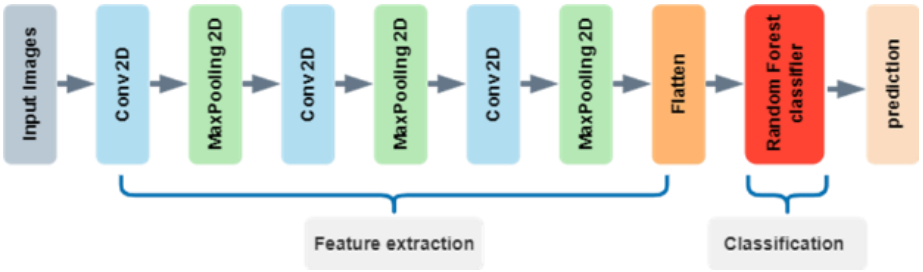

Figure (5): The structure of the CNN-RF model.

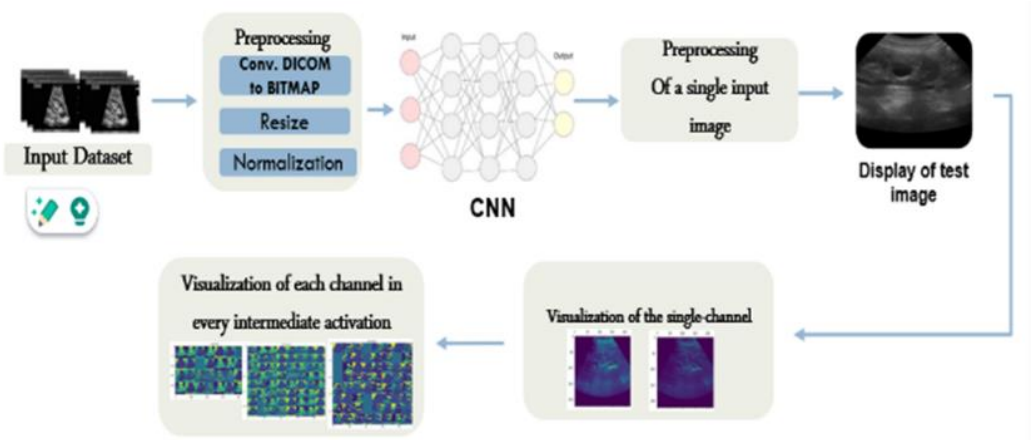

Figure (6): The process of the visualization of intermediate layers activation in CNN

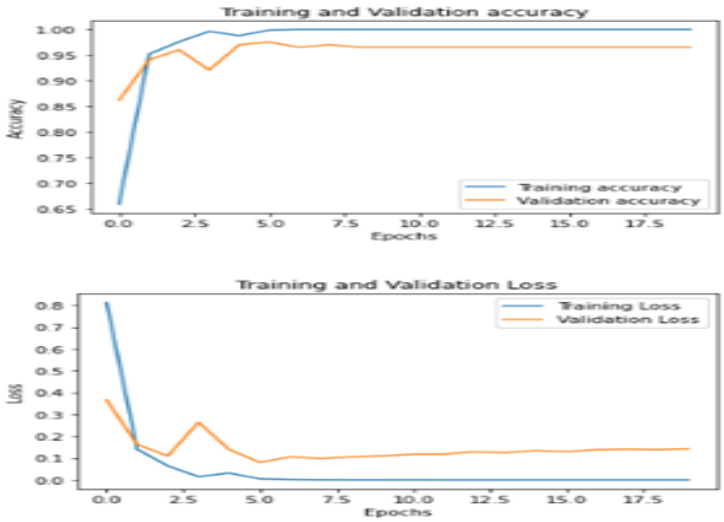

Figure (7): Illustrates the accuracy and loss curve for 20 epochs of the CNN.

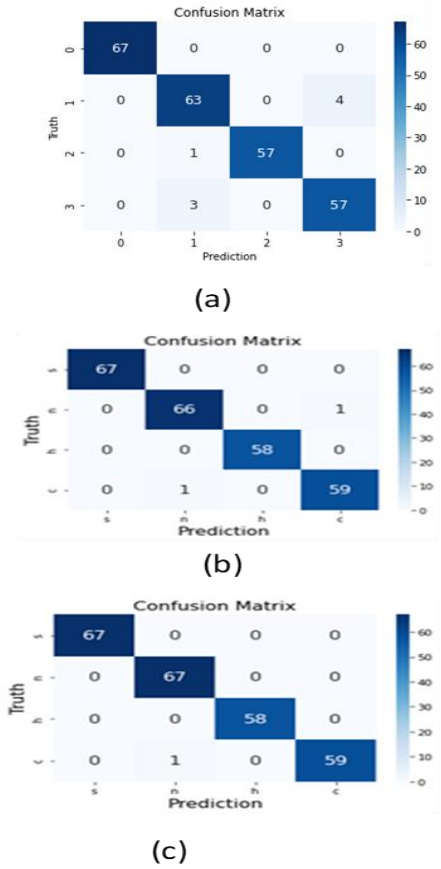

Figure (8): Confusion matrix of (a) CNN, (b) CNN-XGBOOST, (c) CNN-RF.

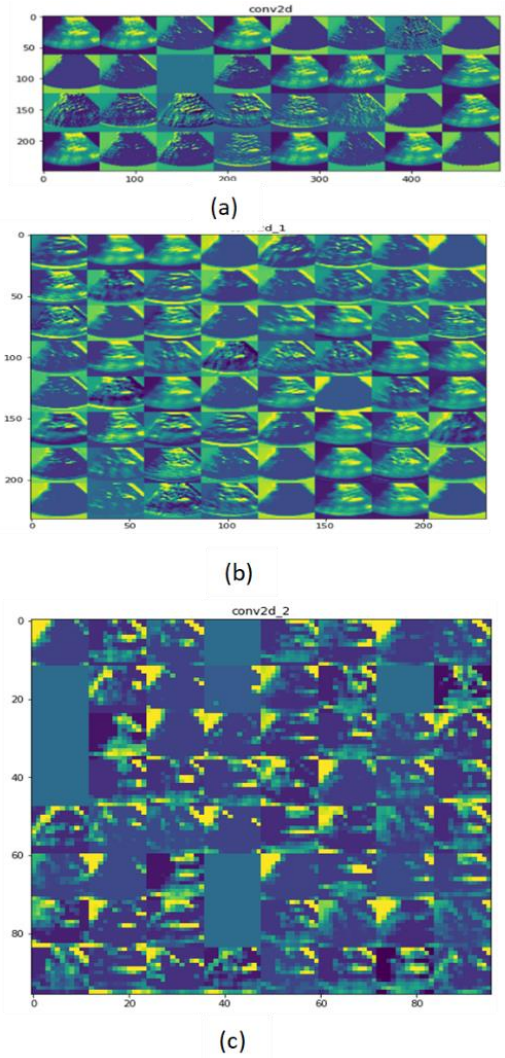

Figure (9): VIA for an input US image in the three convolutional layers of the CNN model: (a) conv1, (b) conv2, (c) conv3.

7. Discussion:

This study developed four models to identify abnormalities in kidney ultrasound images using real data from Iraqi healthcare centers. CNN play a potential role in feature extraction from medical images, and the dense with SoftMax activation

function, RF and XGBoost were used to classify (an unseen dataset of 1260 US images) kidney abnormalities. Several previous studies utilized deep learning models to extract features from medical images, followed by machine learning algorithms for classifying kidney abnormalities. ResNet100 and XGboost were used for the binary classification of 4,505 kidney ultrasound images, achieving an accuracy of 85.6% [18]. A pre-trained, off-the-shelf convolutional neural network (CNN) was used to extract features from the kidney US images. These features were then fed into the SVM classifier to categorize the kidney images into three classes: normal, cystic, and containing stones. The model achieved an accuracy of 91.8% on a performance evaluation. [19]. On three variation datasets, the performance (96.54% accuracy) was obtained using the pre-trained DNN models and SVM for classification. The model divides the kidney's ultrasound pictures into four groups: normal, cyst, stone, and tumor [20]. In this study, CNN model was utilized to identify significant texture features in the images, RF and XGBoost were used for classification, CNN-RF achieved 99.6%, and the accuracy of CNN-XGBoost, and CNN was 97%. **Table 5** shows previous methods used to classify kidney US images in comparison to the proposed model. The advantage of models in this study was automatically detect important features in ultrasound images and classify kidney ultrasound images as cyst, stone, hydronephrosis, and normal.

Table (4): Previous methods in comparison to the suggested approach.

No.	Authors	Methodology	Dataset (Ultrasound kidney images)	Model Accuracy
1	2019, [18]	ResNet100-XGBoost	4,505 images, binary classification	85.6%
2	2020, [20]	Pre-trained DNN models-SVM	images, multi-classification	96.54%
3	2020, [19]	Pre-trained CNN-SVM	1072 images, multi-classification	91.8%
4	Proposed method	CNN-RF, CNN-XGboost, CNN	1260 images, multi-classification	CNN-RF 99.6%, CNN-XGboost 99%, CNN 97%

8. Conclusion:

Kidney diagnostic models were formulated employing a CNN for feature extraction, dense, RF, and XGBoost were used to classify the 1260 kidney US images. Our proposed models achieved better performance than using the CNN model alone. This is because they combine feature extraction with a CNN and classification using Random Forest or XGBoost algorithms, which focus on enhanced performance accuracy. These models possess the potential to serve as an efficacious resolution for the demanding clinical milieu, especially in Iraq. At the same time, taking into consideration the limited accessibility of medical research and diagnostic alternatives. This model was devised to assist radiologists in the analysis procedure and enhance the efficiency of patient care by curtailing the time allocated to interpreting renal images, also this model improves the accuracy of diagnosis systems.

9. References:

[1] A. C. Webster, E. V. Nagler, R. L. Morton, and P. Masson, "Chronic Kidney Disease," *The Lancet*, vol. 389, no. 10075, pp. 1238–1252, Mar. 2017, doi: 10.1016/S0140-6736(16)32064-5.

[2] A. S. Levey *et al.*, "Definition and classification of chronic kidney disease: A position statement from Kidney Disease: Improving Global Outcomes (KDIGO)," *Kidney International*, vol. 67, no. 6, pp. 2089–2100, Jun. 2005, doi: 10.1111/J.1523-1755.2005.00365.X.

[3] Z. M. El-Zoghby *et al.*, "Urolithiasis and the risk of ESRD," *Clinical journal of the American Society of Nephrology : CJASN*, vol. 7, no. 9, pp. 1409–1415, Sep. 2012, doi: 10.2215/CJN.03210312.

[4] V. Patel *et al.*, "miR-17~92 miRNA cluster promotes kidney cyst growth in polycystic kidney disease," *Proceedings of the National Academy of Sciences of the United States of America*, vol. 110, no. 26, pp. 10765–10770, Jun. 2013, doi: 10.1073/PNAS.1301693110.

[5] P. Nuraj and N. Hyseni, "The diagnosis of obstructive hydronephrosis with Color Doppler ultrasound," *Acta Informatica Medica*, vol. 25, no. 3, pp. 178–181, 2017, doi: 10.5455/aim.2017.25.178-181.

[6] K. M. Sternberg, V. M. Pais, T. Larson, J. Han, N. Hernandez, and B. Eisner, "Is Hydronephrosis on Ultrasound Predictive of Ureterolithiasis in Patients with Renal Colic?," *Journal of Urology*, vol. 196, no. 4, pp. 1149–1152, 2016, doi: 10.1016/j.juro.2016.04.076.

[7] H. Diaa AL-rubaie, H. K. Aljobouri, Z. J. AL-Jobawi, and I. Çankaya, "Convolutional Neural Network Deep Learning Model for Improved Ultrasound Breast Tumor Classification," *Al-Nahrain Journal for Engineering Sciences* , vol. 26, no. 2, pp. 57–62, Jul. 2023, doi: 10.29194/NJES.26020057.

[8] P. N. T. Wells, "Ultrasound imaging," *Physics in Medicine and Biology*, vol. 51, no. 13, pp. R83–R98, Jun. 2006, doi: 10.1088/0031-9155/51/13/R06.

[9] K. L. Hansen, M. B. Nielsen, and C. Ewertsen, "Ultrasonography of the kidney: A Pictorial Review," *Diagnostics*, vol. 6, no. 1, pp. 1–18, Mar. 2016, doi: 10.3390/diagnostics6010002.

[10] S. B. Belhaouari and A. Islam, "Deep Learning in Healthcare," in *Lecture Notes in Bioengineering*, Springer Science and Business Media Deutschland GmbH, 2021, pp. 155–168. doi: 10.1007/978-3-030-67303-1_13/COVER.

[11] X. Y. Zhang *et al.*, "Artificial intelligence - based ultrasound elastography for disease evaluation - a narrative review," *Frontiers in oncology*, vol. 13, 2023, doi: 10.3389/FONC.2023.1197447.

[12] P. Hamet and J. Tremblay, "Artificial intelligence in medicine," *Metabolism*, vol. 69, pp. S36–S40, Apr. 2017, doi: 10.1016/J.METABOL.2017.01.011.

[13] K. R. Chowdhary, "Introducing Artificial Intelligence," in *Fundamentals of Artificial Intelligence*, Springer India, 2020, pp. 1–23. doi: 10.1007/978-81-322-3972-7_1.

[14] S. Pattanayak, "Mathematical Foundations," in

Pro Deep Learning with TensorFlow 2.0, Apress Berkeley, CA, 2023, pp. 1–108. doi: 10.1007/978-1-4842-8931-0_1.

[15] A. Chunduru, A. R. Kishore, B. K. Sasapu, and K. Seepana, "Multi Chronic Disease Prediction System Using CNN and Random Forest," *SN Computer Science*, vol. 5, no. 1, pp. 1–13, Jan. 2024, doi: 10.1007/s42979-023-02521-6.

[16] Y. T. Shen, L. Chen, W. W. Yue, and H. X. Xu, "Artificial intelligence in ultrasound," *European Journal of Radiology*, vol. 139, pp. 1–12, Jun. 2021, doi: 10.1016/j.ejrad.2021.109717.

[17] I. Castiglioni *et al.*, "AI applications to medical images: From machine learning to deep learning," *Physica Medica*, vol. 83, pp. 9–24, Mar. 2021, doi: 10.1016/j.ejmp.2021.02.006.

[18] C. C. Kuo *et al.*, "Automation of the kidney function prediction and classification through ultrasound-based kidney imaging using deep learning," *npj Digital Medicine*, vol. 2, no. 1, pp. 1–9, Dec. 2019, doi: 10.1038/s41746-019-0104-2.

[19] P. Kokil and S. Sudharson, "Automatic Detection of Renal Abnormalities by Off-the-shelf CNN Features," *IETE Journal of Education*, vol. 60, no. 1, pp. 14–23, Jan. 2019, doi: 10.1080/09747338.2019.1613936.

[20] S. Sudharson and P. Kokil, "An ensemble of deep neural networks for kidney ultrasound image classification," *Computer Methods and Programs in Biomedicine*, vol. 197, no. 105709, pp. 1–9, Dec. 2020, doi: 10.1016/j.cmpb.2020.105709.

[21] V. M. Raja Sankari, D. A. Raykar, U. Snekhalatha, V. Karthik, and V. Shetty, "Automated Detection of Cystitis in Ultrasound Images Using Deep Learning Techniques," *IEEE Access*, vol. 11, pp. 104179–104190, 2023, doi: 10.1109/ACCESS.2023.3317148.

[22] V. Thambawita, I. Strümke, S. A. Hicks, P. Halvorsen, S. Parasa, and M. A. Riegler, "Impact of Image Resolution on Deep Learning Performance in Endoscopy Image Classification: An Experimental Study Using a Large Dataset of Endoscopic Images," *Diagnostics 2021, Vol. 11, Page 2183*, vol. 11, no. 12, p. 2183, Nov. 2021, doi: 10.3390/DIAGNOSTICS11122183.

[23] M. J. Willemink *et al.*, "Preparing medical imaging data for machine learning," *Radiology*, vol. 295, no. 1, pp. 4–15, Feb. 2020, doi: 10.1148/RADIOL.2020192224/ASSET/IMAGES/LARGE/RADIOL.2020192224.FIG5B.JPEG.

[24] S.Gopal, K. Patro, and K. K. Sahu, "Normalization: A Preprocessing Stage," *arXiv.org*, pp. 20–22, Mar. 2015, doi: 10.17148/IARJSET.2015.2305.

[25] L. A. Shalabi, Z. Shaaban, and B. Kasasbeh, "Data Mining: A Preprocessing Engine," *Journal of Computer Science*, vol. 2, no. 9, pp. 735–739, Sep. 2006, doi: 10.3844/JCSSP.2006.735.739.

[26] C. Wakholi *et al.*, "Deep learning feature extraction for image-based beef carcass yield estimation," *Biosystems Engineering*, vol. 218, pp. 78–93, Jun. 2022, doi: 10.1016/J.BIOSYSTEMSENG.2022.04.008.

[27] A. Jain, M. Pandey, and S. Sahu, "A Deep Learning-Based Feature Extraction Model for Classification Brain Tumor," *Lecture Notes on Data Engineering and Communications Technologies*, vol. 90, pp. 493–508, 2022, doi: 10.1007/978-981-16-6289-8_42/COVER.

[28] S. Q. Salih, A. L. Khalaf, N. S. Mohsin, and S. F. Jabbar, "An optimized deep learning model for optical character recognition applications," *International Journal of Electrical and Computer Engineering*, vol. 13, no. 3, pp. 3010–3018, Jun. 2023, doi: 10.11591/IJECE.V13I3.PP3010-3018.

[29] S. Albawi, T. A. Mohammed, and S. Al-Zawi, "Understanding of a convolutional neural network," in *Proceedings of 2017 International Conference on Engineering and Technology, ICET 2017*, Institute of Electrical and Electronics Engineers Inc., Jul. 2017, pp. 1–6. doi: 10.1109/ICEngTechnol.2017.8308186.

[30] Y. Song *et al.*, "Large Margin Local Estimate With Applications to Medical Image Classification," *IEEE transactions on medical imaging*, vol. 34, no. 6, pp. 1362–1377, Jun. 2015, doi: 10.1109/TMI.2015.2393954.

[31] M. Mirigliano *et al.*, "A binary classifier based on a reconfigurable dense network of metallic nanojunctions," *Neuromorphic Computing and Engineering* , vol. 1, no. 2, p. 024007, Nov. 2021, doi: 10.1088/2634-4386/AC29C9.

[32] T. Chen and C. Guestrin, "XGBoost: A scalable tree boosting system," in *Proceedings of the 22nd ACM SIGKDD International Conference on Knowledge Discovery and Data Mining*, Association for Computing Machinery, Aug. 2016, pp. 785–794. doi: 10.1145/2939672.2939785.

[33] L. Tian, W. Wu, and T. Yu, "Graph Random Forest: A Graph Embedded Algorithm for Identifying Highly Connected Important Features," *Biomolecules*, vol. 13, no. 7, Jul. 2023, doi: 10.3390/BIOM13071153.

[34] H. El Hamdaoui, S. Boujraf, N. E. H. Chaoui, B. Alami, and M. Maaroufi, "Improving Heart Disease Prediction Using Random Forest and AdaBoost Algorithms," *International Journal of Online and Biomedical Engineering (iJOE)*, vol. 17, no. 11, pp. 60–75, 2021, doi: 10.3991/IJOE.V17I11.24781.

[35] P. Sahu, A. Chug, A. P. Singh, D. Singh, and R. P. Singh, "Deep Learning Models for Beans Crop Diseases: Classification and Visualization Techniques," *International Journal of Modern Agriculture*, vol. 10, no. 1, pp. 796–812, Mar. 2021.

[36] S. Rajaraman and S. Antani, "Visualizing Salient Network Activations in Convolutional Neural Networks for Medical Image Modality Classification," *Communications in Computer and Information Science*, vol. 1036, pp. 42–57, 2019, doi: 10.1007/978-981-13-9184-2_4.